JAMES | Journal of Advances in Modeling Earth Systems

RESEARCH ARTICLE
10.1029/2019MS001843

Neighboring Column Approximation—An Improved 3D Thermal Radiative Transfer Approximation for Non-Rectangular Grids

Carolin Klinger[1] and Bernhard Mayer[1]

[1]Lehrstuhl für Experimentelle Meteorologie, Ludwig-Maximilians-Universität München, Munich, Germany

Key Points:
- A new approach of the Neighboring Column Approximation, a fast 3D radiative transfer method is presented
- The method can now be used on non-rectangular grids, and the heating rate bias is reduced
- The method is meant for use in LES models, and computational costs are a factor of 1.5 to 2 compared to a 1D radiative transfer approximation

Correspondence to:
C. Klinger,
carolin.klinger@physik.uni-muenchen.de

Citation:
Klinger, C., & Mayer, B. (2020). Neighboring column approximation—An improved 3d thermal radiative transfer approximation for non-rectangular grids. *Journal of Advances in Modeling Earth Systems*, *12*, e2019MS001843. https://doi.org/10.1029/2019MS001843

Received 30 JUL 2019
Accepted 25 NOV 2019
Accepted article online 28 DEC 2019

Abstract We present a significantly improved version of the Neighboring Column Approximation (NCA 2.0), a fast 3D approximation for the calculation of thermal heating and cooling rates in cloudy atmospheres for large eddy simulation models. The method can now be used on non-rectangular grids, and the heating rate bias in cloudy atmospheres is substantially reduced compared to a 1D solution and the original version of the NCA (NCA 1.0). For different cloud fields the bias is in the range of −5–30% in the 1D case and −2–7% for the NCA 2.0. The calculation of 3D radiative transfer quantities requires horizontal transport of radiation which causes difficulties in the parallelization of numerical models and is computationally expensive. The NCA overcomes this problem and can calculate 3D thermal heating rates at the expense of only a factor 1.5 to 2 higher compared to a 1D radiative transfer approximation. The method uses the fluxes calculated by a 1D radiation scheme and estimates horizontal fluxes using results from neighboring columns. For the estimation of the heating rates from the before estimated fluxes pre-calculated lookup tables of emissivities are used. For the calculation of the heating rates we neglect scattering (independent of the fact if the incoming fluxes consider scattering or not). Inconsistencies made by assumptions for the method are corrected by a correction factor.

Plain Language Summary Radiation drives weather and climate of our planet. Yet radiative transfer is treated poorly in most atmospheric models. A common way to treat radiative transfer in atmospheric models is a so-called independent column approximation. However, this method is known to introduce biases. Especially in today's high-resolution large eddy simulations models, 3D radiative effects become more and more important. This work describes a new and fast approach (Neighboring Column Approximation, NCA) which allows calculating 3D heating and cooling rates in the thermal spectral range in large eddy simulation models. Compared to the previously described method, the new one can also be used on non-rectangular grid, as for example a triangular grid, and it improved in speed and accuracy.

1. Introduction

Emission and absorption of radiation in the atmosphere (also known as heating rates) are an important part of the atmospheric energy balance. In cloudless sky conditions, heating rates are typically in the order of −1 to −2 K day^{-1} (Kelvin per day) while at the interfaces of clouds, they can reach much higher values. The amount of energy of radiative heating is in the same order of magnitude as the release of latent heat and can therefore play an important role in the development of clouds.

Thermal radiative heating is known to affect the evolution of clouds. Cloud top cooling for example is a key driver in maintaining stratocumulus clouds by enhancing turbulent fluxes and maintaining an in cloud circulation which keeps the clouds alive (Wood, 2012, and citations therein). While for stratiform clouds, 1-dimensional (1D) approximations are a sufficient way to describe the radiative heating and cooling rates, finite clouds (e.g., shallow cumulus clouds and cumulonimbus clouds) are affected by 3-dimensional (3D) radiative transfer effects. 1D heating rates are calculated using 1D radiative transfer approximations applied as independent column approximation (ICA), thus taking care of inhomogeneity effects. However, 1D ICA does not allow for horizontal transport of radiation. This horizontal transport of radiation causes enhanced cloud top cooling and additional cloud side cooling, so-called 3D effects, in the thermal spectral range. These 3D thermal heating rates can be as high as several hundred K day^{-1} (Kablick et al., 2011; Klinger & Mayer, 2014) and have been shown to modify cloud circulation and cloud field organization (Guan et al., 1997; Klinger et al., 2017, 2019) of shallow cumulus clouds.

Accurate radiative transfer models (such as Monte Carlo models, e.g., MYSTIC, Mayer, 2009, or SHDOM, Evans, 1998) exist, but their high computational costs prevent their application in cloud models and make new approaches necessary. The "Neighboring Column Approximation" (NCA, Klinger & Mayer, 2016), a 3D approximation for the calculation of thermal heating rates is, next to the "TenStream" (Jakub & Mayer, 2015b, 2015a), one of two fast methods to calculate 3D thermal heating rates and was successfully implemented and applied in different large eddy simulation (LES) models (e.g., UCLA-LES, Stevens et al., 2005, or SAM, Khairoutdinov & Randall, 2003). It can be used in parallelized models and was shown to increase the computational time only by a factor of 1.5 to 2 compared to a 1D radiative transfer approximation in LES. The shown effects of 3D radiative heating rates on the development of shallow cumulus clouds (cloud field organization and cloud circulation) ask for further investigation. So far, the studies investigating 3D effects on cloud development focused on specific cloud types and were carried out in idealized large eddy simulations. With the new version of the NCA we can now calculate 3D effects with more confidence as the bias of the method is reduced. Furthermore, with the possibility to run the NCA in the ICON model (ICON-LEM, Dipankar et al., 2015; Heinze et al., 2017), we can shift to more realistic cases where different cloud types and more realistic time scales are considered. In this paper, we describe a new approach, based on the ideas of the original NCA to calculate 3D thermal heating rates on non-rectangular grids (such as triangular grids). This is an important step, as more and more atmospheric models are developed on non-rectangular grids.

The paper is structured as follows: Section 2 describes the physical background and radiative transfer theory, Section 3 describes the modification of the original NCA for the use on non-rectangular grids, Section 4 shows application and performance of the method, and Section 5 provides a summary and conclusions.

2. Radiative Transfer Theory and Reference Models

In this section we introduce the radiative transfer theory and physical background of our approximation. Furthermore, we describe the reference radiative transfer models/approximations used in this study.

2.1. Radiative Transfer Theory and Heating Rate Calculation

The radiative transfer equation (RTE, Chandrasekhar, 1950) describes the propagation and interaction (scattering, absorption, and emission) of radiation though a medium (e.g., the atmosphere)

$$\frac{1}{\beta_{\text{ext}}}\,\vec{s}\,\nabla L = -L + \frac{\omega_0}{4\pi}\int_{4\pi} p(\Omega',\Omega)\,L(\Omega')\,d\Omega' + (1-\omega_0)\,B(T). \tag{1}$$

β_{ext} is the volume extinction coefficient, L is the radiance in direction $\vec{s}$, ω_0 the single scattering albedo, $p(\Omega',\Omega)$ the scattering phase function, and $B(T)$ is the Planck function at temperature T.

Thermal radiation in the Earth's atmosphere is emitted and absorbed by molecules and particles in the atmosphere as well as the Earth's surface. The basic physics of thermal radiative transfer are described by Planck's law (Planck, 1901) and Kirchhoff's law (Kirchhoff, 1890). Planck's law describes the amount of energy emitted by a black body, depending on the body's temperature and the wavelength. According to Kirchhoff, the emitted or absorbed amount of energy depends on the spectral emission or absorption coefficients which are equal to each other. Scattering, in the thermal spectral range, is of minor importance compared to solar radiative transfer and is therefore often neglected. In this case, the RTE reduces to the "Schwarzschild Equation"

$$\frac{dL}{ds} = \beta_{\text{abs}}\;[B(T) - L]\,, \tag{2}$$

with the absorption coefficient β_{abs} which can be solved analytically (e.g., Liou, 2002).

In the absence of scattering, the transmitted radiance L_{trans} along a path ds can be calculated by using Lambert Beers law:

$$L_{trans} = L_0\;\exp(-\beta_{abs}\;ds). \tag{3}$$

It thus follows that the absorbed radiance along this path L_{abs} equals

$$L_{abs} = L_0\;(1 - \exp(-\beta_{abs}\;ds)). \tag{4}$$

Following Kirchhoff's law, the emissivity equals the absorptivity and the emitted radiance L_{em} is

$$L_{em} = B(T)\;\epsilon, \tag{5}$$

where

$$\epsilon = (1 - \exp(-\beta_{abs}\ ds)) \tag{6}$$

is the emissivity ϵ along the path.

To calculate heating and cooling rates, or fluxes (irradiance, E), radiances must be calculated for various directions and have to be integrated over solid angle. Choosing one specific representative angle μ_{rep} is one way to calculate irradiance and heating rates. For each radiance distribution $L(\mu)$ there is always a μ_{rep} for which the approximation is actually an equality:

$$E = \int_{2\pi} L(\mu, \phi)\ \mu\ d\mu\ d\phi = 2\pi \int_0^1 L(\mu)\ \mu\ d\mu \approx \pi \cdot L(\mu_{\text{rep}}). \tag{7}$$

The absorbed or emitted electromagnetic power per volume (often referred to as heating or cooling rate and measured as change of temperature with time $\frac{dT}{dt}$, [K day^{-1}]), can be written as

$$\frac{dT}{dt} = -\frac{1}{\rho c_{\text{p}}}(\dot{q}_{\text{em}} - \dot{q}_{\text{abs}}) = -\frac{1}{\rho c_{\text{p}}}\nabla\vec{E}_{\text{net}}, \tag{8}$$

with E_{net} defined as the difference of the irradiance in positive and negative directions (horizontally and vertically), ρ is the density of a medium, c_{p} the specific heat capacity of the medium, and $\dot{q}_{\text{em}} - \dot{q}_{\text{abs}}$ emitted minus absorbed power per volume (see, e.g., Liou, 2002).

2.2. Reference Models

For the development of the "Neighboring Column Approximation" on non-rectangular grids and the evaluation of its results we use the Monte Carlo model MYSTIC (see Section 2.2.1). Furthermore, we will compare the improvements of the NCA and the version for non-rectangular grids against the original version of the NCA (Section 2.2.2).

2.2.1. Monte Carlo Model—MYSTIC

As a reference model for the calculation of the 3D thermal heating rates we use the Monte Carlo model MYSTIC (Monte Carlo code for the phYSically correct Tracing of photons In Cloudy atmospheres, Mayer, 2009). MYSTIC is part of the libRadtran radiative transfer package (Emde et al., 2016; Mayer & Kylling, 2005). The specific Monte Carlo methods used for the calculation of the 3D thermal heating rates are described in Klinger and Mayer (2014). The detailed setup of the benchmark simulations will be described in the according section.

2.2.2. Neighboring Column Approximation—NCA

The "Neighboring Column Approximation" (NCA, Klinger & Mayer, 2016) is a fast and accurate method to calculate 3D heating and cooling rates in the thermal spectral range. The approximation considers net fluxes across horizontal box boundaries in addition to the top and bottom boundaries and thus calculates analytically 3D heating rates from 1D fluxes. It makes use of the upwelling and downwelling fluxes from direct neighboring columns only to estimate horizontal fluxes, thus allowing for a parallelized treatment of the radiative transfer in cloud models. The use of neighboring columns is crucial to keep the approximation fast. Otherwise, the general problem that 3D radiation has to propagate over large distances in the horizontal would remain which would break the parallelization in cloud models. The NCA neglects scattering for the heating rate calculation and uses a representative angle of 45° for the propagation of radiation through a grid box (see equation (7)), which can be integrated through the grid box's volume (integration along all paths for one representative angle through a grid box). With these approximations it offers an analytical solution to the 3D radiative transfer problem. The error of the heating rate, due to several approximations made (e.g., neglect of scattering, neighboring column treatment, and the representative angle), depends on the geometry of the cloud field. In general it lies within the range of 5–15%, equally high as for ICA. However, as cloud side heating rates are taken into account by the NCA, the root mean square error is reduced. It was shown that the computational cost are about a factor of 1.5 to 2 higher, compared to a 1D approximation in LES application. This factor depends on the overall performance of the LES and the implementation of the NCA in the specific LES model. For further information, the reader is referred to the work of Klinger and Mayer (2016) and Klinger et al. (2017).

3. Adaption of the NCA on Non-Rectangular Grid

As the development of numerical models advances, grid structures change. Nowadays, a common one in atmospheric research is the triangular grid. In order to make 3D thermal radiative transfer available for those models, we modified our original approach of the NCA. We will refer to the original NCA as *NCA* 1.0 and to the new version as *NCA* 2.0. We tested different approaches and found that there is even a simpler way than the one we used for the *NCA* 1.0. This new approach is not only simpler but also more precise and reduces the above mentioned bias of the *NCA* 1.0 significantly, which is shown later in the paper. We test our new approach again on an rectangular grid and extend the approach to a triangular grid.

3.1. General Idea

NCA 1.0 is a fast solution where absorption and emission are calculated analytically by integrating over a rectangular grid box. The difficulty in applying the NCA to a non-rectangular grid is the integration of the solving equation over a complex volume which causes equations with many terms that are computationally expensive to evaluate. While trying to adapt this approach we found a new way which is (a) simpler and (b) more precise than the integration through a complex volume.

The basic ideas of the *NCA* 1.0 stay the same. Similar to the original version of the NCA, we still use 1D fluxes from the center column under consideration and its neighbors to estimate the 3D heating and cooling rates and we still neglect scattering. However, we omit integration of the solving equations over a complex volume by making use of pre-calculated lookup tables of the emissivity. Our new approach includes the following main steps which apply to all grid structures:

- Estimation of the incoming irradiance E at top, base and side faces of a grid box from 1D upward and downward irradiance of the neighboring columns and the column under consideration.
- Calculation of tables of spectral emissivity for grid boxes with various optical thickness and aspect ratios.
- Calculation of correction factors to correct the neglect of scattering and approximations in the estimation of the incoming irradiances and the spectral emissivity.

For these three steps we create lookup tables and fit functions. The lookup tables depend on optical depth and aspect ratio. This way we make sure that they can be used for any kind of atmospheric composition and for different grid setups (e.g., grid box size) as long as the grid type (rectangular, triangular, etc.) does not change. The lookup tables are based on full 3D radiative transfer calculations with our Monte Carlo model MYSTIC. A detailed description of the individual steps is shown in the following and in Appendix A. We will illustrate the method on a rectangular grid (for reference) and a triangular grid.

3.2. Method

3.2.1. Heating Rate Calculation

We assume that calculation of the irradiance from the radiance is known (equation (7)). Therefore, it follows with equations (4), (5), and (7) that the absorbed or emitted power per volume, of a grid box face, can be calculated as

$$\dot{q}_{\mathrm{abs,l}} = E_l \, \epsilon_l \, \frac{A_l}{V}, \tag{9}$$

$$\dot{q}_{\mathrm{em,l}} = B(T) \, \pi \, \epsilon_l \, \frac{A_l}{V}, \tag{10}$$

where E_l is the incoming irradiance, $B(T)$ the Planck emission at temperature T of the grid box, A_l the grid box face surface area, V the grid box volume, and ϵ_l the emissivity of the grid box. l represents a grid box face. This equation can be transformed for the NCA by applying the equation for each face (n_{faces}) of a grid box individually and calculating the sum of all contributions:

$$\dot{q}_{\mathrm{abs,nca}} = \sum_{l=0}^{n_{faces}} E_l \, \epsilon_l \, \frac{A_l}{V}, \tag{11}$$

$$\dot{q}_{\mathrm{em,nca}} = \sum_{l=0}^{n_{faces}} B(T) \, \pi \, \epsilon_l \, \frac{A_l}{V}. \tag{12}$$

In the limit of infinite optical thickness (and hence emissivity equal to 1), these equations are identical to equations (14) and (18) of Klinger and Mayer (2016).

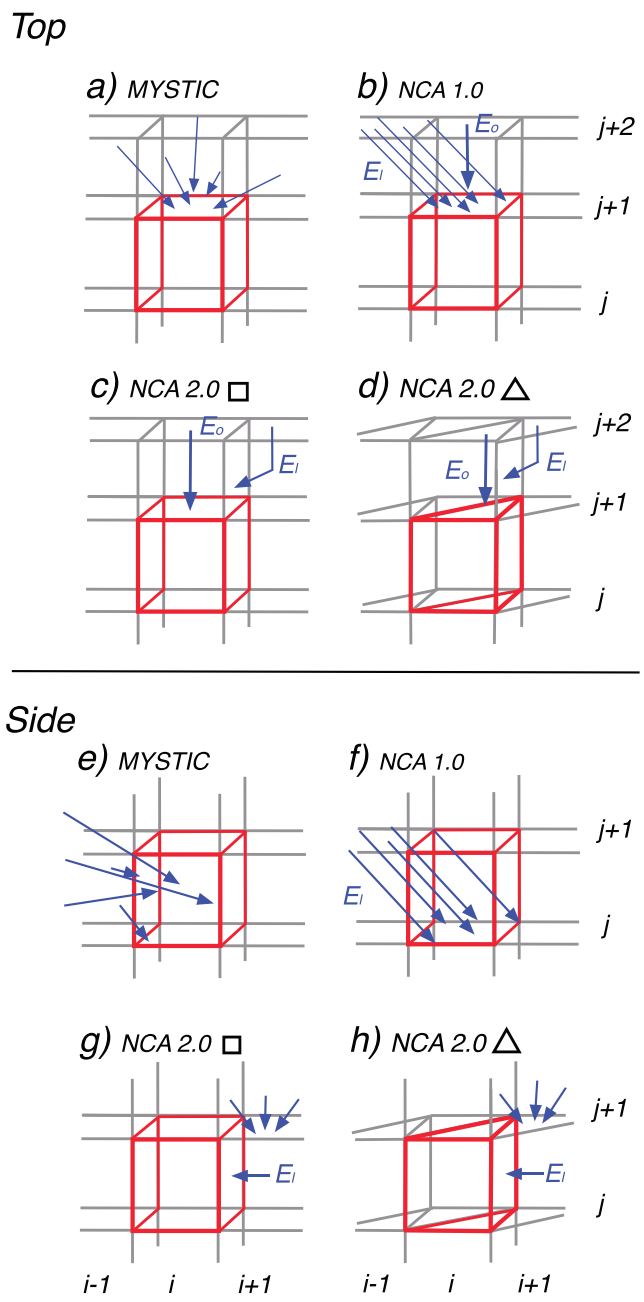

Figure 1. Schematic figure of the incoming irradiances for a full 3D approach (a), the *NCA* 1.0 (b), and the *NCA* 2.0 on rectangular (c) and triangular grid (d) at the side and top faces of a grid box. Only one side direction is shown in each case.

Thus, the heating rate $dTdt^{-1}$ in K day^{-1} becomes

$$\begin{aligned}\frac{dT}{dt} &= -\frac{1}{\rho c_p}(\dot{q}_{em} - \dot{q}_{abs}) \\ &\approx -\frac{1}{\rho c_p}(\dot{q}_{em,nca} - \dot{q}_{abs,nca}) \\ &= -\frac{1}{\rho c_p}\left(\sum_{l=0}^{n_{faces}} \varepsilon_l \left(B(T)\,\pi - E_l\right)\frac{A_l}{V}\right).\end{aligned} \tag{13}$$

In the following we will describe how the emissivities ε_l, the incoming irradiances E_l, and the correction factor are calculated.

3.2.2. 3D Heating Rate Calculation

For the calculation of $dTdt^{-1}$ (equation (13)), one needs to know the incoming irradiance and the optical thickness of the grid box under consideration. Figure 1 shows schematically the difference between a full 3D approach (*a* and *e*) the *NCA* 1.0 (*b* and *f*) and the *NCA* 2.0 (*c*, *d*, *g*, and *h*). Only one side direction is shown to keep the figure simple and only the downwelling fraction is shown. Please note that for each rectangular based grid box 4 side directions and for each triangular based grid box 3 side directions have to be considered. Before going into detail how irradiance and emissivity are calculated for *NCA* 2.0 we briefly want to summarize how this is done in a full 3D calculation and for the *NCA* 1.0 respectively and what the problems are when generalizing the main idea of the *NCA* 1.0 for different grids.

We first focus on a full 3D calculation. Figure 1 shows schematically the incoming irradiance which hits a top face ($j+1$) of a grid box (*a*) and a side face of a grid box (*e*, between j and $j+1$) in a full 3D calculation. Different directions have to be taken into account for the calculation of the incoming irradiance and in the following the heating rate. Furthermore, radiation emerges from further away than the shown boxes. This makes solving 3D radiative transfer computationally expensive.

For the *NCA* 1.0 (Figures 1b and 1f) we simplified this problem by choosing on representative angle of 45° for the calculation of the incoming irradiance (and the heating rate). For *NCA* 1.0, the incoming irradiances at top/bottom and the side face of a grid box is calculated separately. The top/bottom irradiance (level $j+1$, Figure 1) is calculated as an average of 4 incoming neighboring irradiances at level $j+2$ from the neighboring columns and the irradiance of the center column, propagating with an angle of 45° through the grid box of the layer between $j+1$ and $j+2$ (Figure 1b). (Please note again that only one direction is shown in Figure 1.) Using a combination of the center column irradiance and the four neighboring irradiances in the top/bottom case assures that the effect of nearby clouds is taken into account. This irradiance then propagates through the grid box in question (red box) to calculate the absorbed amount of the irradiance.

The side contribution to the heating rate is a complex integral where the irradiance at level $j+1$ is propagating through the neighboring grid box $i-1$ and the grid box under consideration (Figure 1f, red box) and the absorbed amount is calculated in one step. For more details, the reader is referred to Klinger and Mayer (2016), Section 2.3.

Rather than analytically evaluating the integral when different grid shapes are considered we calculated the incoming irradiance from top/bottom and side faces and the emissivity (ε_l) separately in the *NCA* 2.0. Finally, we correct the uncertainties introduced by different assumptions with a correction factor.

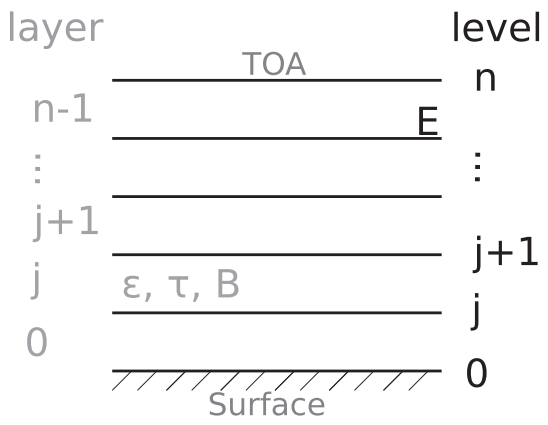

Figure 2. Schematic figure to illustrate the level/layer convention used in the description of the NCA in the following. Irradiance E is a level quantities, emissivity (ϵ), optical depth (τ) and Planck function B are layer quantities.

Before proceeding, Figure 2 provides a schematic overview of the level/layer convention and the main quantities involved in the following description of the method. Irradiance is defined on levels, Planck function, emissivity and optical depth are defined on layers.

3.2.3. Spectral Emissivity/Absorptivity

We start with the calculation of the spectral emissivity ε_l for each grid box face l. The emissivity (equation (6)) varies with optical thickness and the aspect ratio of a grid box, respectively. The optical thickness again varies for different wavelengths. Therefore, we calculate the emissivity in dependence of the optical depth. As the optical depth is a function of the distance that radiation passes in a volume, it considers the aspect ratio of the grid box as well. In application, the optical depth of a grid box is calculated for each spectral band (or wavelength) individually. For each spectral band (or wavelength) we can thus get the corresponding emissivity from the lookup table. Thus, constructing a lookup table based on optical depth assures that we consider all dependencies of the emissivity if it is applied spectrally. Emissivity equals absorptivity, following Kirchhoff.

$$\epsilon = \alpha. \tag{14}$$

We calculate absorptivity and store it in lookup tables. The absorptivity varies for incoming irradiance depending on the direction of the incoming irradiance. In case of a cube, the absorptivity is on average the same for all directions (or cube faces) of the incoming irradiance. This changes however for a flat, rectangular shaped, grid box where the absorptivity is higher for the downwelling and upwelling component of the irradiance as opposed to the incoming irradiance from side directions (see Figure 3 left and right column in comparison). Essentially it is a function of the grid box volume that is passed by the incoming irradiance.

We focus on a rectangular grid first: To take multiple directions of the irradiance and therefore optical thickness of one grid box into account we calculate a representative absorptivity for each face, depending on the optical thickness of a grid box, thus avoiding integration over multiple directions. By optical thickness we mean the optical thickness perpendicular to a grid box face. We vary the aspect ratio of the grid box. Thus, we get different optical depths in all three directions (τ_x, τ_y, τ_z).

The absorptivity is then calculated as the fraction of the absorbed irradiance ($abs_l(\tau_x, \tau_y, \tau_z)$ through one grid box face (l) compared to the incoming irradiance E_l of one grid box face.:

$$\epsilon_l(\tau_x, \tau_y, \tau_z) = \frac{abs_l(\tau_x, \tau_y, \tau_z)}{E_l}. \tag{15}$$

The dependence of the thus calculated absorptivity on one grid box face makes it (a) usable within the NCA framework (see equation (13)) where we calculate the contribution to the heating rate for each grid box face and (b) assures that we account for different aspect ratios. In application, this means that for each grid box we get for each grid box face a specific emissivity from the lookup table, based on the grid box face's aspect ratio (ζ) and the optical depth (rectangular grid: $\zeta = dzdx^{-1}$ for top/base contributions, $\zeta = dxdz^{-1}$ or $\zeta = dydz^{-1}$ for side contributions; triangular grid: $\zeta = dzh^{-1}$ for top/base contributions and $\zeta = dxdz^{-1}$ or $\zeta = dydz^{-1}$ for side contributions).

We calculate the absorptivities with our 3D Monte Carlo model MYSTIC (for the specific setup, please see Appendix A.1). Separate lookup tables are required for each specific grid face, depending on the grid shape. While one lookup table is sufficient for a rectangular grid two setups are required for the triangular grid—one for the simulation of the top (base) face absorptivities and one for the calculation of the side face absorptivities (see Figures 3b and 3c). This is necessary as the face shape changes (triangle vs. rectangle) and therefore also the geometry of the absorbing volume. Again, the reader is referred to Appendix A.1 for the specific Monte Carlo setup). The general idea stays the same: We calculate the absorptivity in a triangular base face grid box depending on varying optical thickness. Note that for the triangular grid, a equilateral triangle is assumed in our case. This introduces small uncertainties if the shape of the triangle changes

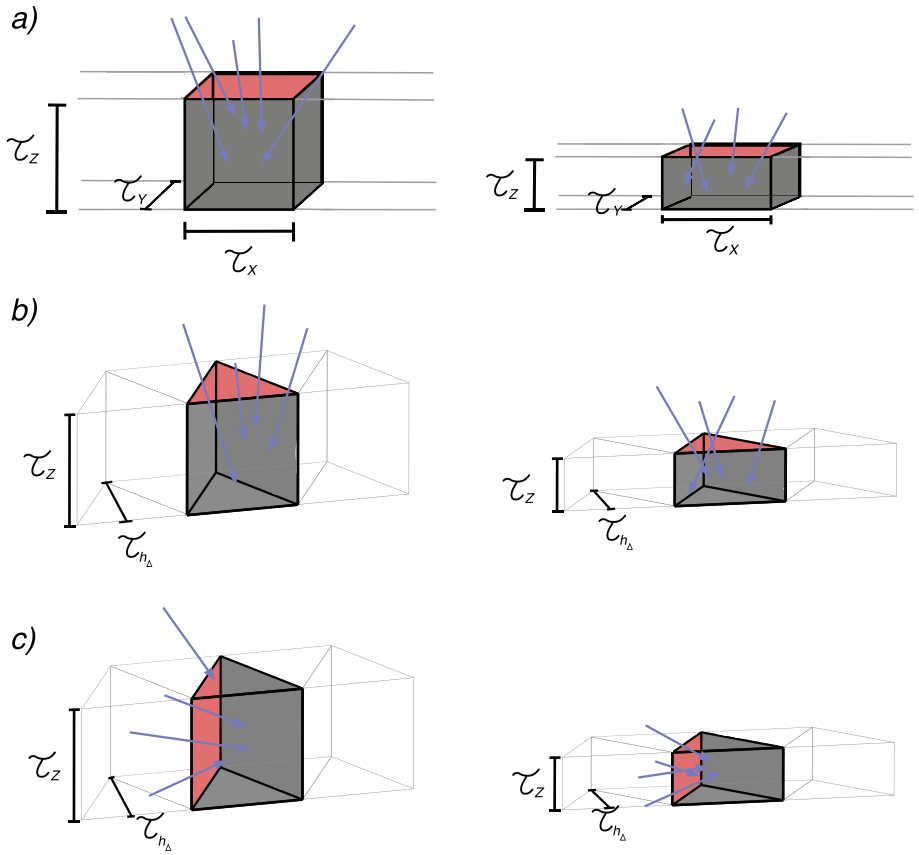

Figure 3. Setup for estimating the spectral emissivity/absorptivity depending on the optical thickness and aspect ratio. The upper figure (a) shows the setup for a regular grid, the lower two figures show the setup for top (b), and side (c) emissivities/absorptivities for a triangular grid.

substantially (see Section 4); however, the triangles vary only slightly in the ICON model (ICON-LEM, Dipankar et al., 2015; Heinze et al., 2017) for which we intend the method to work. By adding a further dimension, the lookup tables could of course be calculated for a variety of triangle shapes, if necessary.

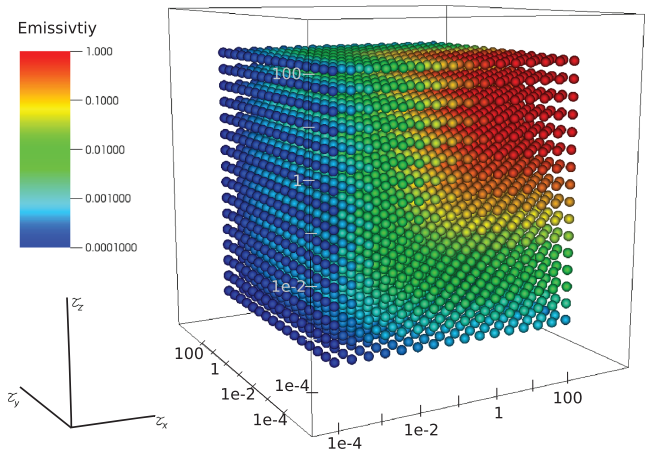

Figure 4. Visualization of the 3D lookup table of the emissivities/absorptivities for a rectangular grid, depending on the three optical thickness (τ_x, τ_y, τ_z).

The absorptivities of the lookup table for the regular grid are shown in Figure 4. For small optical thickness, the absorptivity is low, while it converges towards 1 for high optical thickness.

3.2.4. Incoming Irradiance

The next step focuses on estimating the incoming irradiance E_l for each grid box face. Similarly to the *NCA* 1.0, we use 1D irradiance of the center column and the neighboring columns to calculate the 3D heating rate. We still separate contributions from the top/bottom face and side faces of a grid box. To avoid the complex integration through a volume we estimate with the help of Monte Carlo simulations the contribution of center and neighboring irradiance to the total incoming irradiance of a grid box.

Estimation of the Top and Bottom Irradiance

First, we will focus on the incoming irradiance at top ($E_{top,j+1}$) and bottom ($E_{bot,j}$) of the grid box under consideration (i,j). The irradiance from $n_{side}+1$ columns (the center column and n_{side} side columns) contributes to the incoming irradiance at top (base) face. Based on the results of the *NCA* 1.0, the incoming irradiance is a combination of the center column irradiance and the average of the n_{side} irradiances. Not using the center

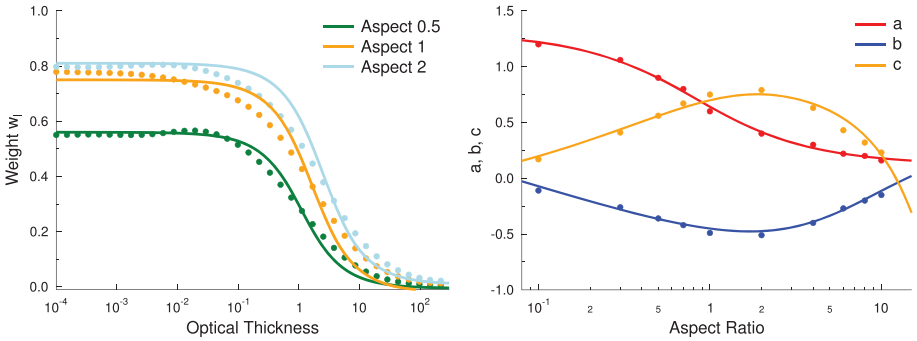

Figure 5. Weights for the incoming radiances at the top face of a rectangular grid cell for three aspect ratios (0.5, 1, and 2) depending on the optical thickness and aspect ratio as well as the coefficients a(ζ), b(ζ), and c(ζ). The dots represent the Monte Carlos results, and the solid line shows the fit using equation (19).

irradiance alone but also accounting for the n_{side} neighboring column irradiances assures that nearby clouds which modify the irradiances contribute to the result. The amount of the center and neighbor irradiance at level $j+1$ (j) to the incoming top (base) irradiance depends on the optical thickness and the aspect ratio of the grid box above (below) (see Figure 1). If the grid box above (below) the one in question is optically thick, most of the irradiance will originate from the grid box directly above (below) the one under consideration. If the optical thickness of the grid box above (below) the one under consideration is thin, the neighboring irradiances contribute as well. The contribution of the neighboring irradiances also depends on the aspect ratio. A very flat grid box will still receive most of the irradiance from the grid box directly above (below), but for a very tall one, the neighbors gain more weight. We therefore calculated weights w_l (with l being the index of the top (0) or base face (1)) dependent on the optical thickness and the aspect ratio (ζ) of the upper ($j+1$) (lower ($j-1$)) grid box which give us the contribution of the averaged side irradiance. The weights $(w(\tau,\zeta)_l)$ for one grid box face are calculated as the fraction of the transmitted irradiance entering the grid box under consideration compared to the incoming irradiance E_{in} at ($j+1$, top case/$j-1$, bottom case):

$$w(\tau,\zeta)_l = \frac{trans(\tau,\zeta)}{E_{in}}. \tag{16}$$

It therefore follows that the contribution of the center column irradiance ($E_{dn,0,j+1}$ or $E_{up,1,j}$) is $(1-w(\tau,\zeta)_l)$, which means if the the optical depth of the grid box above ($j+1$) or below ($j-1$) is high, the transmission is low, thus the weight $w(\tau,\zeta)_l$ is low and the center irradiance contributes most (and the other way round). Thus, the total incoming irradiance at top/bottom can be calculated as follows:

$$E_{top,j+1} = (1-w(\tau_{j+1},\zeta)_0)\cdot E_{dn,0,j+1} + \; w(\tau_{j+1},\zeta)_0 \; \frac{\sum_{l=2}^{n_{side}} E_{dn,l,j+1}}{n_{side}}, \tag{17}$$

$$E_{bot,j} = (1-w(\tau_{j-1},\zeta)_1)\cdot E_{up,1,j} + \; w(\tau_{j-1},\zeta)_1 \; \frac{\sum_{l=2}^{n_{side}} E_{up,l,j}}{n_{side}}. \tag{18}$$

$E_{dn,0,j+1}$ and $E_{up,1,j}$ are the center column downwelling and upwelling irradiance, $E_{dn,l,j+1}$ and $E_{up,l,j}$ those of the side columns, respectively. The specific setup of the Monte Carlo simulations can be found in Appendix A.2. For the weights, we fitted an *arctan* function (for a variety of aspect ratios and optical thickness) to the data for both grids (the rectangular and triangular grid):

$$w(\tau,\zeta)_l = b(\zeta)\cdot arctan\,(\tau\cdot a(\zeta)\,) + c(\zeta). \tag{19}$$

The coefficients $a(\zeta)$, $b(\zeta)$, and $c(\zeta)$ slightly differ for the two grids. For the rectangular grid the coefficients depend on the aspect ratio $\zeta = dz/dx$ and follow again *arctan* functions. The dependence on aspect ratio was fitted as follows:

$$a(\zeta) = -0.76\cdot arctan(1.21\cdot\zeta) + 1.31,$$

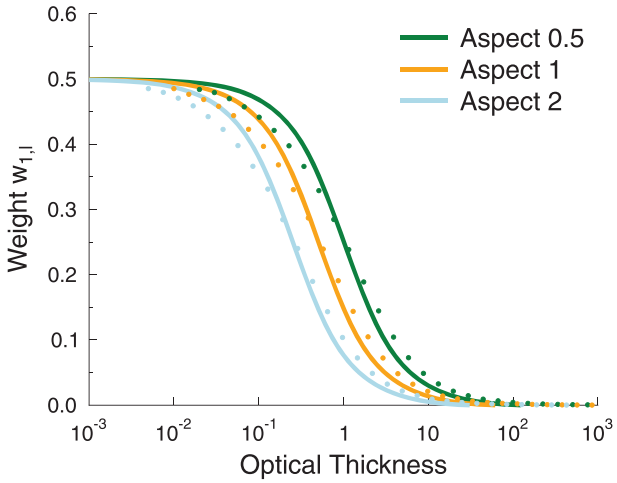

Figure 6. Weights ($w_{1,l}$) for three aspect ratios (0.5, 1, and 2) for the incoming side irradiances correction in dependence of the optical thickness.

$$b(\zeta) = 8.08 \cdot \zeta^{0.028} + 0.01 \cdot \zeta + arctan(0.13 \cdot \zeta) + 7.49,$$

$$c(\zeta) = 1.55 \cdot \zeta^{0.44} - 0.25 \cdot \zeta + arctan(-0.3 \cdot \zeta) - 0.31.$$

For the triangular grid the coefficients $a(\zeta)$, $b(\zeta)$, and $c(\zeta)$ are slightly different. Here, the aspect ratio is defined as $\zeta = dzh^{-1}$, where h is the height of the triangle:

$$a(\zeta) = -0.75 \cdot arctan(1.29 \cdot \zeta) + 1.21,$$

$$b(\zeta) = -7.98 \cdot \zeta^{0.027} - 0.01 \cdot \zeta + arctan(0.11 \cdot \zeta) + 7.36,$$

$$c(\zeta) = 1.46 \cdot \zeta^{0.49} - 0.25 \cdot \zeta + arctan(-0.29 \cdot \zeta) - 0.12.$$

Please note that h is not the distance between the layers j and $j+1$, but the height of the triangle as shown for the optical depth $\tau_{h_\triangle}$ in Figure A4.

As can be seen form the coefficients $a(\zeta)$, $b(\zeta)$, and $c(\zeta)$, the fraction of incoming irradiance varies slightly between the rectangular and triangular grid because the number of neighboring columns and the surface area of the top face is different. An example for three aspect ratios of the fit functions is shown in Figure 5 for the rectangular grid. If the center grid box has a high optical thickness, $w(\tau, \zeta)_l$ converges to zero and only the center irradiance contributes to the incoming irradiance. For low optical thickness, the center irradiance contributes less than the average of the n_{side} neighboring irradiances. It can also be seen from Figure 5 that the fit does not always match exactly the Monte Carlo results. This discrepancy is compensated by the correction factor that is applied at the end (see Section 3.2.5).

Estimation of the Side Irradiance

For the *NCA* 1.0 we use the side irradiance at the level boundary of a grid box under consideration and integrate it through the side grid box and the grid box under consideration to estimate how much of the irradiance is absorbed (Figure 1f). Similar to the top (base) contribution, this integral becomes very complex for non-rectangular girds. We therefore estimate again with the help of Monte Carlos simulations (see Appendix A.2) the fraction of the side irradiance that enters a grid box. The underlying physics for the estimation of the weighting factors for the side irradiances are the following: If the surrounding atmosphere of a grid box is optically thin, most of the irradiance hitting a side face of a grid box originates from the level above (j+1, downwelling case) or below (j, upwelling case) of the grid box (Figure 1). If the surrounding atmosphere is optically thick, the irradiance originates mostly from the layer of the grid box (j). This can be seen from equation (20), which shows the equation for the downwelling irradiance E_{dn} which is the sum of the incoming irradiance from level $(j+1)$ and the emission of the layer itself (j). The first term contributes most if the optical thickness τ_j is low, while in case of high optical thickness the Planck term of the layer contributes most to $E_{dn,j}$.

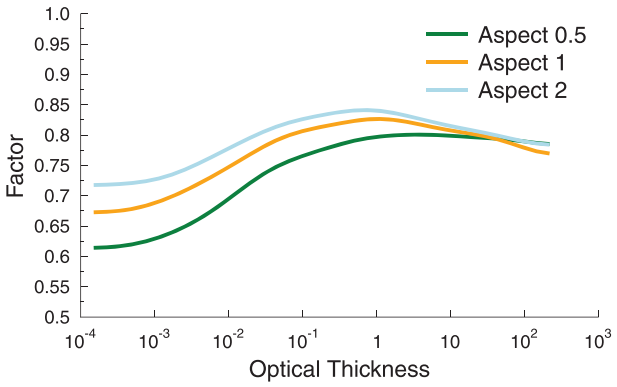

Figure 7. Correction factors accounting for uncertainties in the estimation of the incoming irradiance, the approximated emissivity and the neglect of scattering. The factors scale the heating rates of grid boxes of high optical thickness towards the real heating rate results of an isolated cuboid grid box. Shown here are the correction factors for aspect ratios 0.5, 1, and 2 for the side face correction of the triangular grid boxes.

$$E_{dn,j} = E_{dn,j+1} \cdot exp(-\tau_j) + B(T_j) \cdot \pi \cdot (1 - exp(-\tau_j)). \quad (20)$$

To avoid complex integrals, we use the irradiance at the upper and lower boundaries of a grid box under consideration and estimate the side irradiance contribution as weighted contribution of the irradiance at the upper and lower levels of the layer in question:

$$E_{l,side} = w_{1,l} \cdot E_{l,j} + w_{2,l} \cdot E_{l,j+1}, \quad (21)$$

where l corresponds to one of the side face directions.

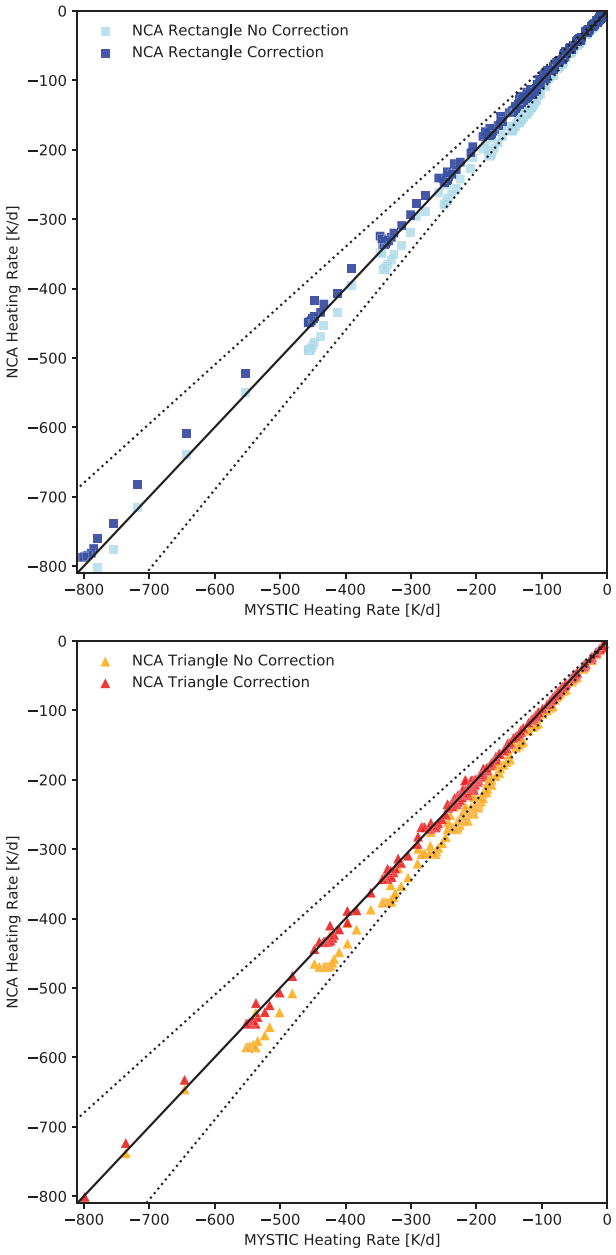

Figure 8. Heating rate results calculated with the *NCA* 2.0 and compared to MYSTIC benchmark results of isolated cuboid (top) and triangular (bottom) grid boxes. In both figures we show the results with and without the application of the final correction factor. The dashed lines show the ±15% interval.

It thus follows that for low optical thickness, irradiances contribute equally from both levels, for high optical thickness from the second layer (where the Planck term of the neighboring grid box dominates). An example for three representative aspect ratios is shown in Figure 6. For both grids (rectangular and triangular), the side face area is a square. Thus, no differentiation for the weights between the two grids is necessary. The weights are found to follow again an *arctan* function:

$$w_{1,l} = 0.32 \cdot arctan(-1.96 \cdot kabs \cdot dz) + 0.5$$
$$w_{2,l} = 1 - w_{1,l}. \tag{22}$$

3.2.5. Correction Factor

As a final step, we calculate correction factors. This is necessary to correct the approximated treatment of incoming irradiance and emissivity, and the neglect of scattering in the calculation of the heating rate. These factors were determined by comparing the results of MYSTIC calculations of heating rates for varying aspect ratios and optical thickness (which can be considered as the truth) to the results of the *NCA* 2.0. The factor is the ratio of the two results and is simply multiplied to the resulting heating rate (either top/base or side contribution from dT/dt, equation (13)). The correction factors were estimated for the top (base) and side contributions separately. The factors are stored in lookup tables. The correction factor is shown for aspect ratios 0.5, 1, and 2 in Figure 7 for the side correction of the triangular grid. For a detailed description of the calculation of the factor, please see Appendix A.3.

Figure 8 shows a comparison of the heating rates for isolated grid boxes from MYSTIC simulations and the *NCA* 2.0 results for both grid types, with and without the correction factor. With the correction factor, the heating rates of MYSTIC and the *NCA* 2.0 match very well (with an average difference of 3%). Without the correction factor, the *NCA* 2.0 overestimates cooling on average by 15%.

4. Application

4.1. Performance of the NCA in Realistic Cloud Fields

We finally test the *NCA* 2.0 in a set of LES cloud fields and compare the results to full 3D Monte Carlo calculations and 1D ICA results. Additionally, we show a comparison to the *NCA* 1.0 version. We present three different cloud field examples in the following and discuss the performance of the method. For the cloud fields we use different aspect ratios and resolutions as well as different cloud types. The three cloud fields are shown in Figures 9a–9c. We chose a nearly overcast stratocumulus case (dx = 40 m, dz = 10 m, van der Dussen et al., 2013) and two cumulus cases (dx = 75 m, dz = 50 m, Klinger et al., 2019, and dx = 100 m, dz = 30 m, Klinger et al., 2017). The Monte Carlo simulations were performed using the backward variance reduction methods for thermal heating rates described by Klinger and Mayer (2014). We use 1,000 photons per spectral band and grid box which keeps the uncertainty below 1%. The correlated-k method of Fu and Liou (1992) is used for spectral integration.

Figures 10a–10d show in addition a cross section of the heating rates of cloud field of Figure 9c at the black marked area for MYSTIC (a), ICA (b), *NCA* 1.0 (c), and *NCA* 2.0 (d) and the difference between ICA and MYSTIC (e), *NCA* 1.0 and MYSTIC (f), *NCA* 2.0 and MYSTIC (g), and *NCA* 1.0 and *NCA* 2.0 (h). These cross sections show the gain but also the limitations of in applying the NCA instead of a 1D approximation. The full 3D Monte Carlos simulation (a) shows a cooling in the whole cross section. Comparing this to the 1D approximation (b) one can see the missing cloud side cooling below cloud top (left and right cloud) and an overestimation of the cloud base warming (for all four clouds) which is a result of the missing horizontal transport of radiation (the loss of radiation through cloud sides). The *NCA* 1.0 and *NCA* 2.0 perform much

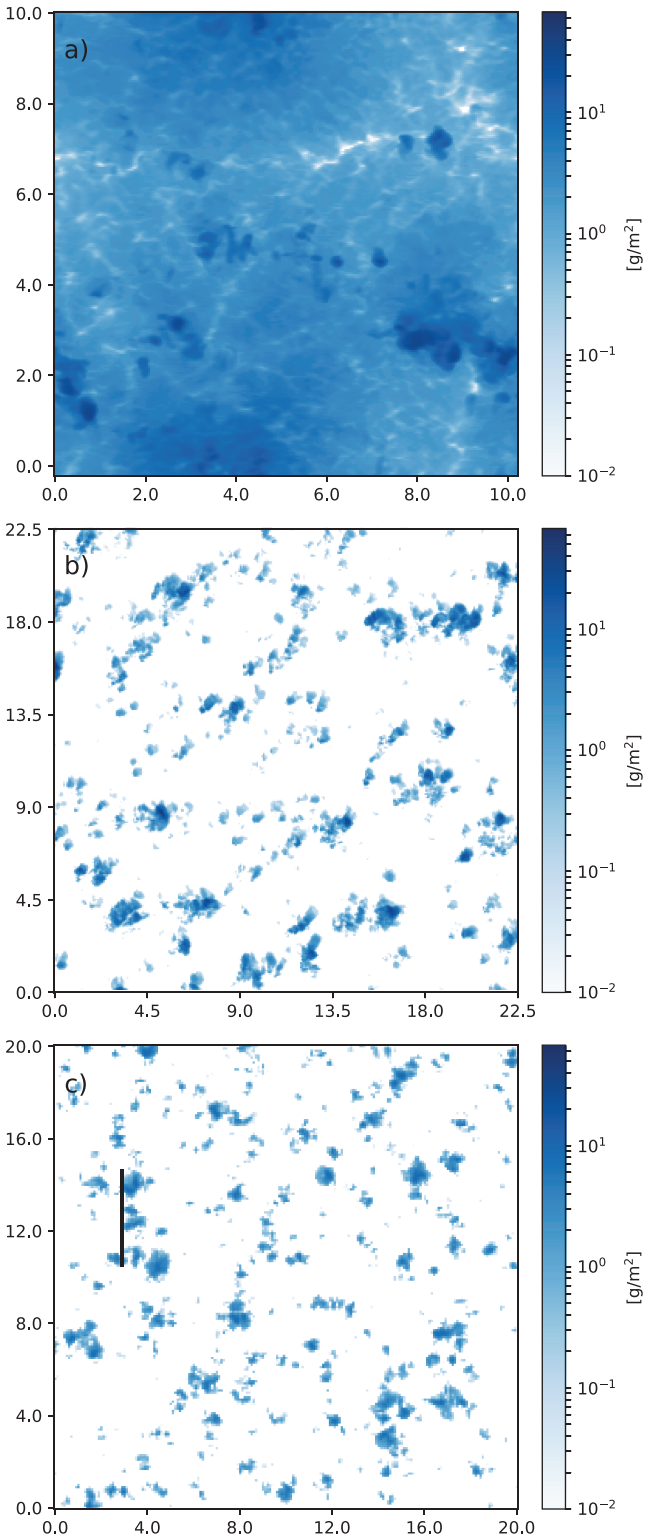

Figure 9. Liquid water path of three different cloud fields: (a) stratocumulus, (b) cumulus case 1, and (c) cumulus case 2 cloud field. The black line indicates the region where cross sections of the heating rates are shown in Figure 10.

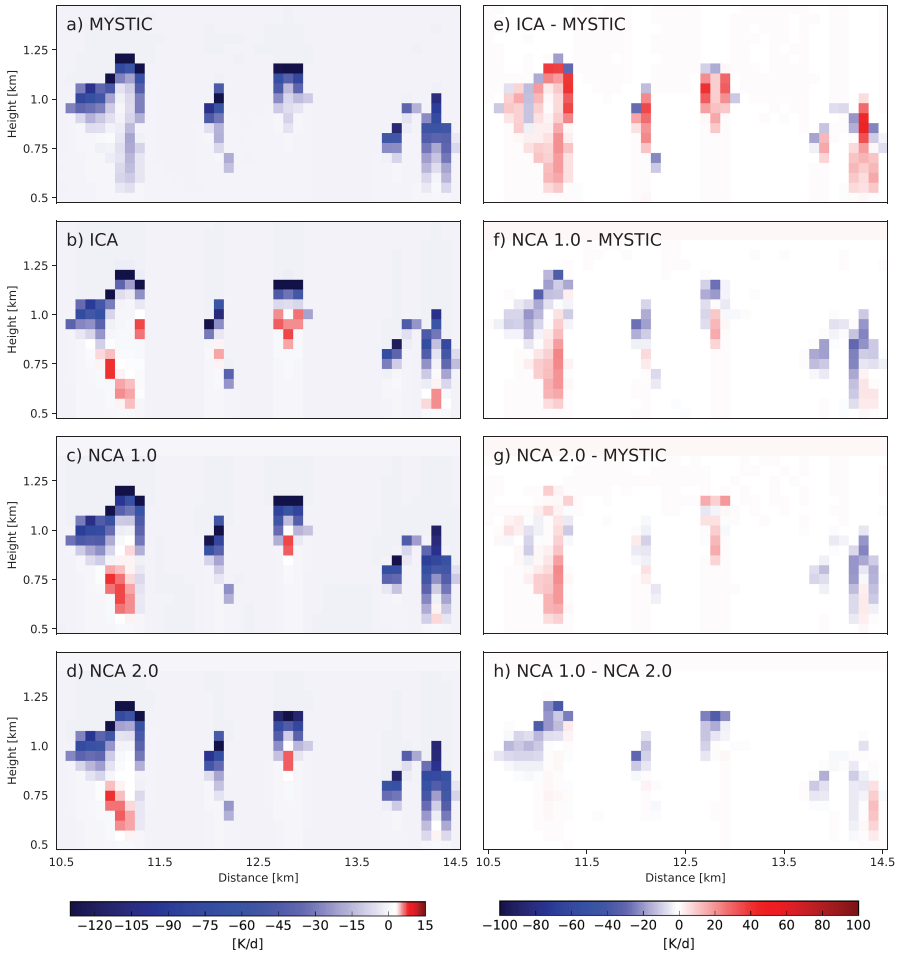

Figure 10. Cross section of the heating rates in the marked region of Figure 9c. The left column shows the total heating rates calculated with MYSTIC (a), ICA (b), NCA 1.0 (c), and NCA 2.0 (d). The right column shows the differences between ICA, NCA 1.0, NCA 2.0, and MYSTIC (e–g) as well as both NCA versions (h).

better than the 1D approximation. Cloud side cooling is calculated for most of the grid boxes and the base warming is reduced. However, one can also see the limitations of the NCA: due to the use of one neighboring column which allows for the parallelization of the method in LES application, radiation cannot be emitted from further in the cloud than one column (see left cloud, second column from right) and in the still too high cloud base warming. This becomes more apparent in the difference plots. The cooling of ICA is reduced in comparison to MYSTIC. Both NCA versions calculate the stronger 3D cooling but overestimate the 3D cooling in comparison to MYSTIC. Comparing both NCA versions (h) shows that *NCA* 2.0 is improved as it cools less than *NCA* 1.0. For more details, the reader is again referred to Klinger and Mayer (2016). Overall, however, the NCA performs much better than a standard 1D approximation which will be shown in the following in a more statistical analysis.

For the comparison with the *NCA* 2.0 on triangular grid, we use the same cloud fields and calculated our benchmark results on the standard rectangular grid, because MYSTIC can not handle non-rectangular grids. We therefore transform the rectangular grid of our test cases to a triangular grid by simply splitting each rectangular grid box into two triangular ones. These triangles are not equilateral triangles, but isosceles triangles. This results in a small error in the application which will be discussed later in the text. We then calculate the heating rates of each of these isosceles triangles and average the two belonging grid boxes to one rectangular grid box and compare this result to the Monte Carlo benchmarks.

Figure 11 shows a 2D histogram of the heating rates of all cloudy grid boxes of the stratocumulus cloud field. The first histogram (upper left) compares 1D ICA heating rates to full 3D Monte Carlo results. As expected, for this stratiform case, the 1D approximation works well. The overall bias in the cloud field is about −5.8%.

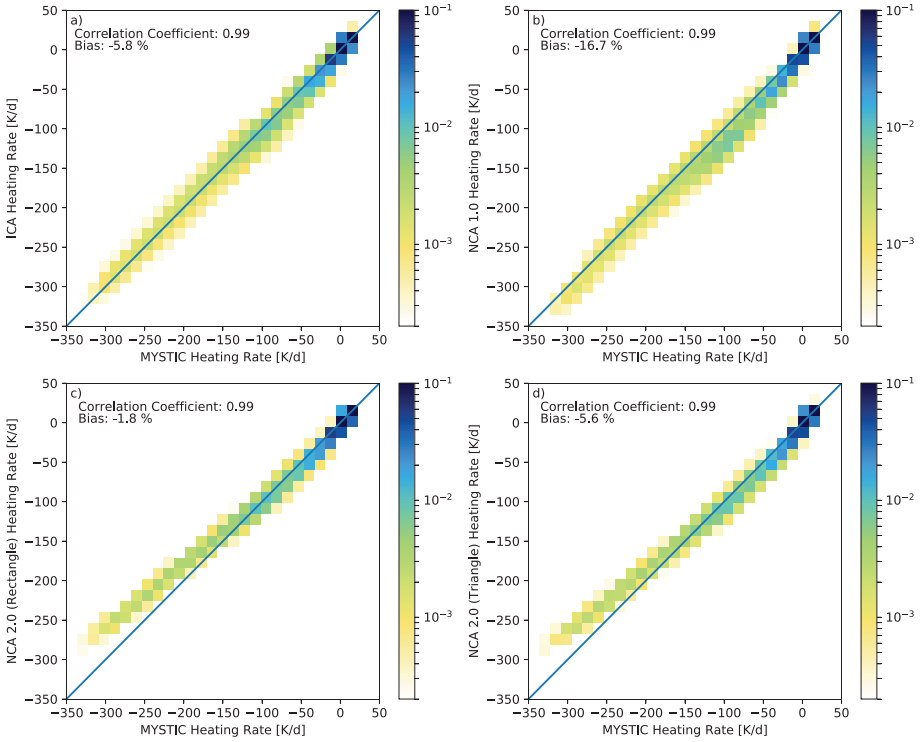

Figure 11. Scatter plot of heating rates of a stratocumulus case. Only cloud grid boxes are evaluated. We compare 1D ICA to 3D Monte Carlo (MYSTIC), NCA 1.0 to MYSTIC, and two application of the NCA 2.0 (rectangular grid and triangular grid) to MYSTIC. Each dot is displayed with a opacity. The denser the dots, the more often the heating rate occurs.

The following three figures of the panel show the *NCA* 1.0 results compared to MYSTIC (upper right). The pixel-by-pixel deviation is smaller; however, the bias increases to more than −16%. This overestimation of the cooling by this approximation is known (Klinger & Mayer, 2016), especially in stratiform cases. The two lower figures show the results of the *NCA* 2.0 applied on a rectangular grid (left) and on triangular grid (right). Both applications also show that the heating rate pixel-by-pixel deviation is much smaller. The bias in the cloud field is substantially reduced compared to *NCA* 1.0 and also reduced compared to the 1D ICA results. The correlation coefficient is equally high. One feature of the *NCA* 2.0 is the underestimation of peak cooling rates (however, these values do not occur frequently; please note the log-colorbar of Figure 11). This feature results from the correction factors that were estimated for isolated grid boxes. We will see later that this feature does not occur for cumulus cases (which can be considered more like an isolated grid box). Table 1 shows in addition the bias for the whole cloud field (including clear sky) and the cloud side grid boxes only. For the stratocumulus case, the bias is in the same order of magnitude as the 1D bias for *NCA* 2.0

Table 1
Relative Bias [%] of the Heating Rates in the Three Different Cloud Fields and Subsets of the Cloud Fields

Cloud type	Analysis	NCA 1.0	NCA 2.0 Rect.	NCA 2.0 Tri.	ICA
Stratocumulus	Total scene	−17.0	−2.3	−6.2	−6.0
	Cloudy pixels	−16.7	−1.8	−5.6	−5.8
	Side pixels	−66.0	−49.1	−54.9	−42.7
Cumulus 1	Total scene	−13.3	−3.4	−10.3	6.3
	Cloudy pixels	2.2	6.5	7.3	29.5
	Side pixels	−5.6	0.2	−7.6	−11.9
Cumulus 2	Total scene	−7.6	1.2	−0.8	8.7
	Cloudy pixels	−6.8	4.7	5.4	15.1
	Side pixels	−7.9	−2.3	2.3	41.4

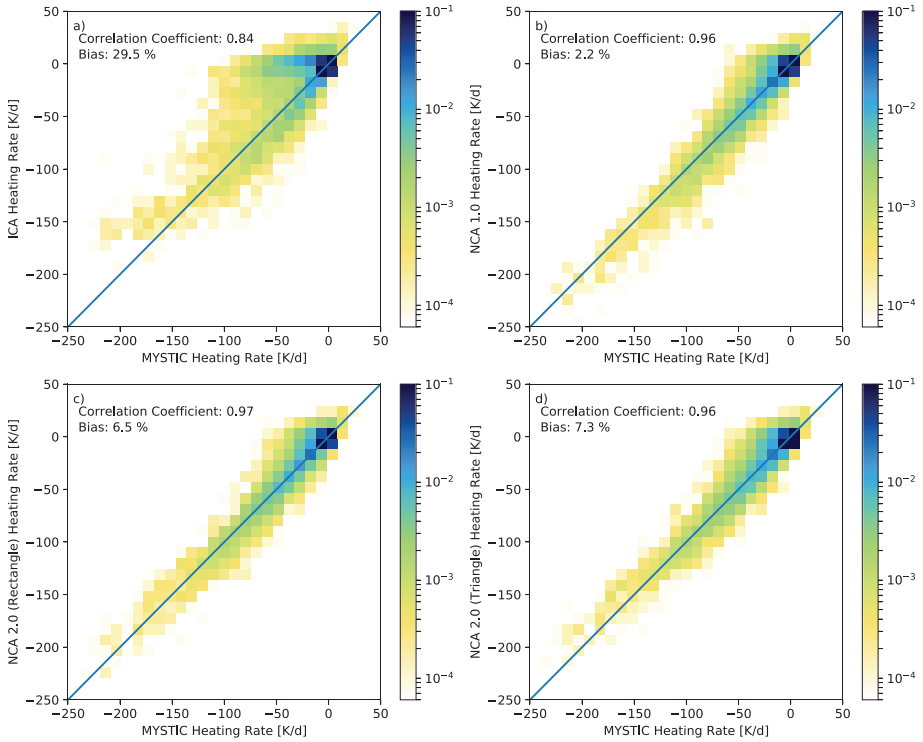

Figure 12. Same figure as Figure 11 but for cumulus 1.

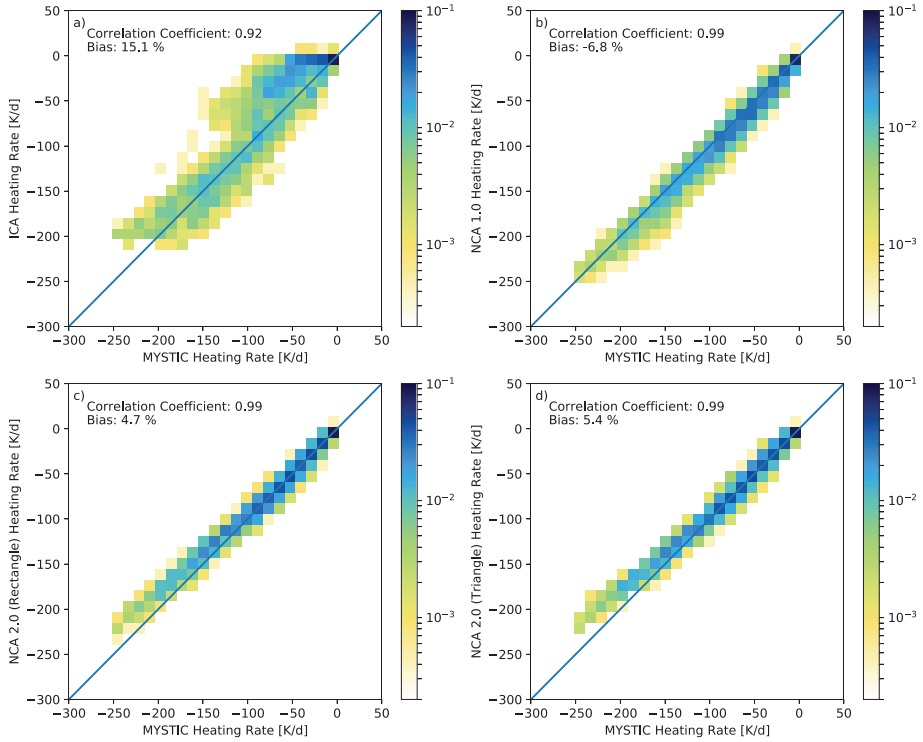

Figure 13. Same figure as Figure 11 but for cumulus case 2.

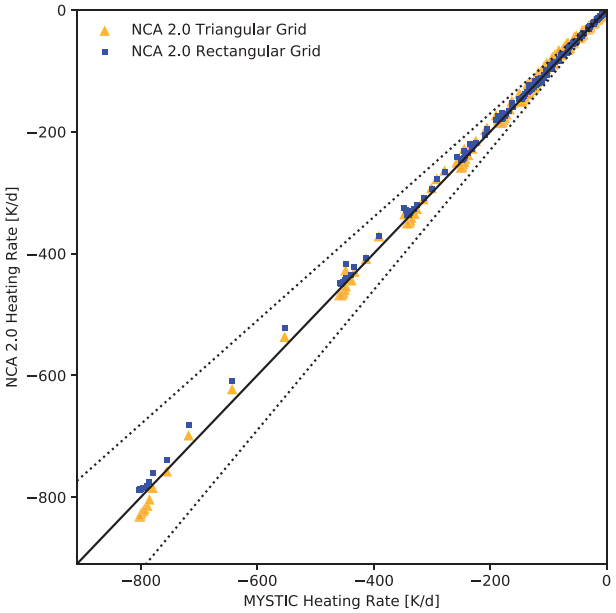

Figure 14. Comparison of heating rates calculated with the NCA 2.0 and MYSTIC. Blue dots show the comparison of the NCA 2.0 on a rectangular grid an MYSTIC; the yellow triangles show the results for the NCA 2.0 with spitted rectangular grid and the triangular solver. A cold bias compared to the NCA 2.0 on rectangular grid is found for low heating rates (low optical depth), because the pre-calculated lookup tables are optimized for nearly equilateral triangles but right-angled triangles are used in this application.

on triangular grid and reduced for *NCA* 2.0 on rectangular grid and is substantially reduced compared to *NCA* 1.0.

Our next case is the first cumulus case. Again, we see that *NCA* 2.0 reduces the bias in the cloud field, in cloudy grid boxes, and also at cloud sides (the specific 3D effect) substantially compared to 1D ICA and also the *NCA* 1.0 (Table 1). *NCA* 2.0 for triangular grids has again a higher bias compared to *NCA* 2.0 for rectangular grid. The 2D histogram (Figure 12) shows again a smaller pixel-by-pixel deviation of the heating rates for all *NCA* applications. The correlation coefficient improves for the NCA. What has to be noted for the cumulus cases are the blue grid boxes which cumulate around 0 $Kday^{-1}$ for the ICA/MYSTIC comparison (upper left). These heating rates are mostly cloud side heating rates, and it is nicely shown by this histogram that the *NCA* can calculate those heating rates much better.

Our last example (Figure 13), the second cumulus case shows similar features as have been explained for the other two examples (smaller pixel-by-pixel deviation of the heating rate and better calculation of the cloud side heating rates, reduced bias and improved correlation coefficient).

For the interpretation of the results of *NCA* 2.0 (on triangular grid), it has to be noted that we used a cloud field on rectangular grid and split the grid boxes. The cold bias in the total field (Table 1) is an artifact of the optimization of the lookup tables for equilateral triangles (see Section 3.2.1) and which become right-angled, isosceles triangles in this application. Indeed, when even comparing the isolated grid boxes and performing the *NCA* 2.0 simulations as used in the cloud fields and comparing them to MYSTIC, we see that warm and cold bias occurs at different magnitudes of the heating rates (which relates to different emissivities) see Figure 14). For heating rates below −200 K day^{-1} we find a cold bias, while above that value the bias changes. We expect the results of the *NCA* 2.0 on triangular grid to shift towards the results of the *NCA* 2.0 on rectangular grid in an application on a real triangular grid.

The bias (clear sky and cloudy areas combined) is reduced compared to NCA 1.0 for the NCA 2.0 in both the rectangular and the triangular application. The overall reduction of the bias (compared to NCA 1.0 and also compared to ICA) is an important issue in application in an LES. Otherwise, the system would be systematically cooled or warmed too much. As for cloudy and cloud side grid boxes, the heating rates here are more relevant for locally correct heating and cooling at the clouds. Our main focus here is the improvement in comparison to ICA which is still the standard treatment for radiative transfer in LES. For

the stratocumulus case shows an improvement compared to the *NCA* 1.0. Compared to ICA, the *NCA* 2.0 perfromes equally well, or better if the total scene and the cloudy pixels are concerned. For the cloud side pixels it should be noted that those are very few in number.

4.2. Computational Time

The *NCA* 1.0 (Klinger & Mayer, 2016) was shown to be a computationally fast 3D radiative transfer solver. In LES application, the computational time increased by a factor 1.5–2 compared to a simulation with a 1D radiative transfer scheme. This factor can vary slightly, depending on the implementation into the LES model.

The *NCA* 2.0 (also not yet implemented into an LES) is expected to run with a similar efficiency. Off-line simulations on the above shown cloud fields showed that the computational time of the *NCA* 2.0 was even reduced compared to the *NCA* 1.0 performance. The time needed for the 3D calculation (after the calculated 1D fluxes) could be reduced by nearly 30–40% for the different cloud fields (all simulations performed on one CPU on a standard office computer; Intel(R) Xeon(R) CPU E5-2630 v4 @ 2.20GHz).

5. Conclusions

We present a new approach for the Neighboring Column Approximation, a fast method for the calculation of 3D thermal heating rates in cloudy atmospheres. With the advancing development of atmospheric models, flexible methods which can be used on structured and non-rectangular model grids are necessary. We therefore modified our original approach (Klinger & Mayer, 2016) to make the NCA usable on non-rectangular grids, like the triangular grid of the ICON model. The method still makes use of the calculated 1D fluxes of the neighboring column of a grid box to estimate the 3D heating rate. However, due to the complexity of integrating the former solving equations on non-rectangular grid box shapes, we modified the original approach which is now based on the use of pre-calculated factors and lookup tables to estimate (a) the amount of a 1D flux entering a grid box, (b) the emissivity and absorptivity of a grid box of specific shape and optical thickness, and (c) finally to correct the thus received result.

It could be shown that the method, applied both on a regular rectangular grid and an non-rectangular triangular grid in LES cloud fields, substantially reduces the relative bias of the heating rates compared to commonly used 1D radiative transfer heating rates and also compared to the original version of the NCA. Furthermore, the method itself (also not yet applied in an LES) reduces the computational time compared to the original NCA. For the former, the computational time was shown to be a factor of 1.5 to 2 in LES application compared to ICA.

Thermal cooling has been shown to have a significant impact on the mesoscale circulation and mesoscale organization of these cloud fields and on the development of individual clouds (e.g., Bretherton & Blossey, 2017; Klinger et al., 2017; Naumann et al., 2017; Seifert et al., 2015). With this new version of the NCA and the possibility to run it in the ICON model, studies of in a more realistic framework, including many different cloud types can be made. It thus offers the possibility to investigate, next to small scale impacts, the broader picture and a possible impact on weather/climate.

Appendix A: Setup for MYSTIC Simulations

A.1. Calculation of the Spectral Emissivity/Absorptivity

Rectangular Grid

For the calculation of the spectral emissivity/absorptivity, which depends on the optical thickness and the aspect ratio, we chose the following setup: We use a very simple setup with one grid box. The temperature is set to 0 K everywhere except for the surface under consideration. The surface serves therefore as black body source (E_l in equation (15) and Figure A1) while all other areas are non-emitting. The absorptivity is then calculated as the absorbed irradiance of the grid box based on one black body emitted irradiance divided by the black body emitted irradiance at the specific temperature (see equation (15)). 10,000,000 photons are traced which assures us a stable result with a standard deviation of less than 0.05%.

The lookup table depends on the optical depth in all three dimensions. We chose one representative path through a grid box for each dimension (perpendicular to the face of the grid box) as reference for the optical thickness. The optical thickness range is between 0.0001 and 100. The increments are increased by a factor

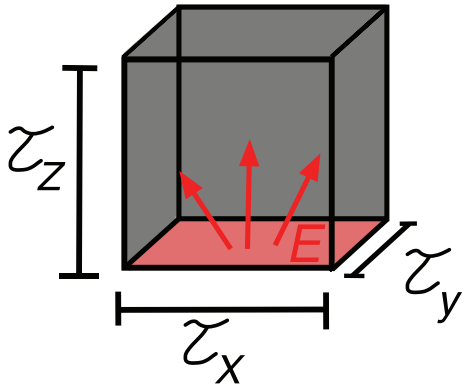

Figure A1. Schematic figure of the MYSTIC setup to calculate the emissivities/absorptivities for a rectangular grid. The surface serves as source of the irradiance. The absorbed irradiance is calculated for the grid box.

of 2.5 which results in 16 entries per dimension. We thus assure that for low optical depth where thermal radiative transfer is more sensitive to changes, the optical depth is better resolved than for high optical depth where thermal radiative transfer approaches saturation. The range of the optical depth is chosen in a way that for low optical depth the transmission is nearly 100% (99.99% if the photons would pass the grid box perpendicular to the face) and approaches zero for the upper bound of the lookup table. Although the aspect ratio is not an entry in the lookup table, the combination of optical depth in the three dimensions implies that different aspect ratios of the grid box are taken into account. For example, having an optical depth of 0.0001 in x and y and of 100 in z corresponds to a stretched grid box with an aspect ratio ($dzdx^{-1}$) of 100,000 (a value that one will not find in an atmospheric model but assures us that the lookup table covers all possibilities). In application, a linear interpolation in three dimensions is performed to get the corresponding emissivity/absorptivity for a specific grid box optical depth.

Triangular Grid

The calculation of the absorptivities for triangular grid follows the same idea; however, as our Monte Carlo model uses a rectangular grid we construct one by creating a triangular prism from small regular grid boxes. Our total domain consists therefore of $50 \times 50 \times 1$ grid boxes (see Figure A2). We use the incoming flux at one face of the prism (red area) as source. All other surface pixels are set to 0 K. The optical thickness of the surrounding atmosphere and the temperature are set to zero. The optical thickness of the prism is varied between 0.0001 and 100 (in the same intervals as for the rectangular grid), but we have two reference distances now instead of three. We use equilateral triangles as base face of the prism which works well for the ICON model. We use the height of the base triangle (τ_h) as one reference path, and the height of the prism as the second reference path (τ_z). We thus reduce the lookup table to two dimension; however, the calculation of the height of the base triangle includes in some degree the third dimension.

As already mentioned in the main text, two different setups are necessary for the calculation to differentiate between top (base) and side absorptivities, because the area of the top (base) face and the side faces are different and therefore the passed volume. For the side face absorptivities, we flip the prism by 90° . Otherwise we perform the same simulations. We use 400,000 photons per pixel. The standard deviation of the calculated absorptivities is again less than 0.05%.

In application, we perform a 2-dimensional interpolation to get the corresponding emissivity/absorptivity for a specific grid box optical depth.

A.2. Calculation of the Fraction of the Incoming Irradiance

As we use 1D irradiance from an independent column solution (see Figure 1) as incoming irradiance for the calculation of heating rates, we need to estimate how much of the irradiance of the center column and the neighboring columns contributes to the overall incoming irradiance of each grid box face. We use sets of idealized simulations with our Monte Carlo model MYSTIC to determine the top (base) and side contributions.

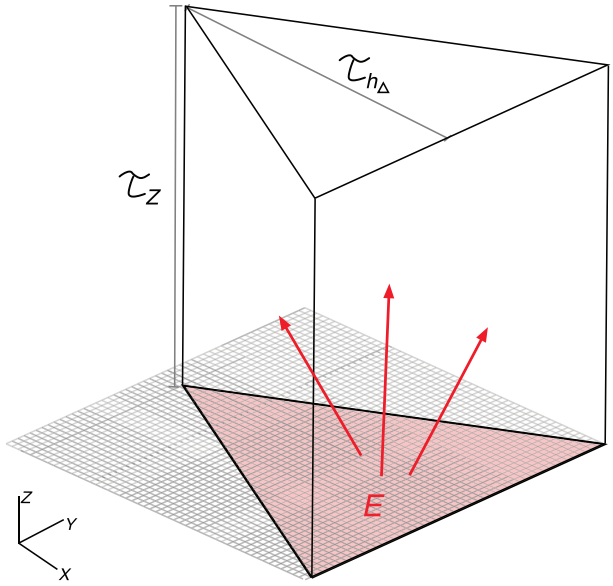

Figure A2. Schematic figure of the MYSTIC setup to calculate the emissivities/absorptivities for a rectangular grid.

Top/Base Irradiance

To get the weights, we calculated the transmitted irradiance arriving at a of a fully absorbing grid box (dark gray, infinite optical thickness τ_{inf}, in Figure A3). The atmosphere itself is non-emitting/non-absorbing (temperature was set to zero, τ_{atm}) in layer $j+1$. The surrounding area in layer j (Figure A3) is fully absorbing but non-emitting. The radiation source is a layer where the temperature was set to 288.2 K except for the part of the center grid box for which the incoming irradiance was estimated. We thus estimate, depending on the optical thickness of the center grid box (light gray, τ) and the aspect ratio how much irradiance of the neighboring columns reaches the grid box in question (dark gray, τ_{inf}). The fraction of the emitted irradiance (at $j+1$) and the transmitted irradiance of the grid box (at j) is our weight for the contribution of the neighboring irradiances. It follows that the weight for the center irradiance is $1-w$. We neglect inhomogeneities in the optical thickness of the surrounding atmosphere. This, however, is partially taken into account in the application by averaging the side column irradiances as shown in equation (17) which have passed the specific inhomogeneous volumes. The setup and calculations are similar for the rectangular and the triangular grid, only the grid shapes changes. The simulations are performed with 1,000,000,000 photons.

Side Irradiance

The calculation of the weights is again performed with 3D Monte Carlo simulations for varying optical thickness (thus also accounting for different aspect ratios). The temperature was set to zero except for one side contribution at the upper level (see Figure A4). Depending on the optical thickness of the atmosphere (τ_{atm}) we calculated the transmitted irradiance arriving at the grid box in question (see Figure A4, gray grid box, fully absorbing) and divide it by the emitted irradiance E. As the shape of the side face is the same for a rectangular and a triangular grid, the weights can be used for both grid types.

$$w = \frac{trans}{E}. \tag{A1}$$

A.3. Calculation of the Correction Factor

The correction factors were calculated by comparing the spectrally integrated heating rates of isolated cuboid grid boxes from 3D MYSTIC simulations in a realistic background atmosphere to the results of the *NCA* 2.0. The factors are calculated for top/base and side contributions to the heating rate separately. The factors are simply multiplied to the heating rate top/base or side result. We used the correlated-k method of (Fu & Liou, 1992) for the spectral integration. The background atmosphere is the U.S. Standard Atmosphere (Anderson et al., 1986). The surface albedo is set to zero.

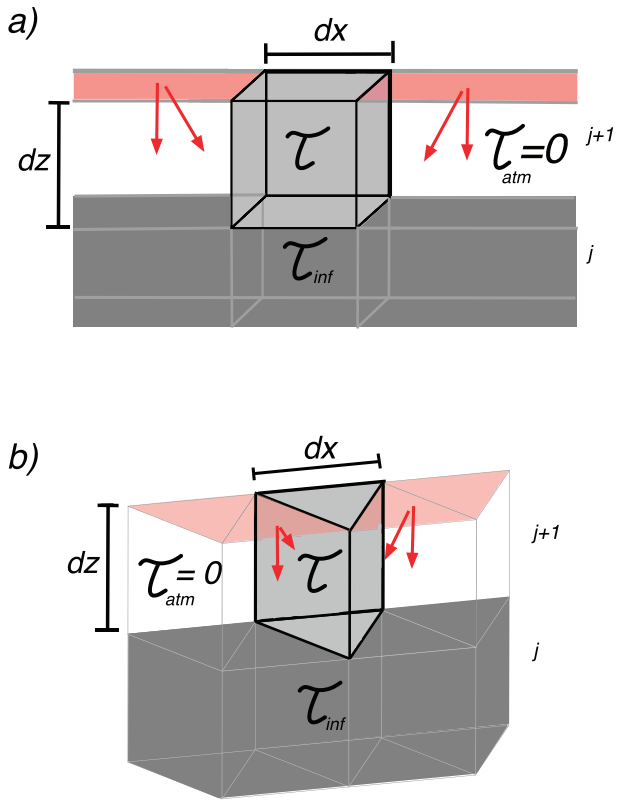

Figure A3. Schematic figure of the MYSTIC setup for the estimation of the top irradiance weights: (a) rectangular and (b) triangular grids. We calculated the transmitted irradiance arriving at grid box j and vary the aspect ratio and the optical thickness of the grid box above.

For the rectangular grid (top/base) we vary the aspect ratio ($dzdx^{-1}$) of the grid box from 0.1 to 10 in the following intervals: 0.1, 0.2. 0.3, 0.5, 1.0, 2.0, 3.0, 5.0, and 10. These aspect ratios cover typical values in atmospheric models. The optical depth of the grid box is varied between 0.0001 and 300 again the increments are increased by a factor of 2.5; 1,000,000 photons are used. The atmosphere surrounding the grid box in the grid box layer is set to be a black body wherefore the side contributions of emission and absorption to the heating rate cancel each other out. The remaining heating rate only originates from the top/base face. The ratio of the 3*DMYSTIC* result to the *NCA* 2.0 results is the correction factor.

The factor for the side contribution follows a similar setup, except that the grid box above and below the one in questions are considered to be black bodies. In this case, the aspect ratio is defined as $dxdz^{-1}$.

For the triangular grid we follow the same main idea. Similar to the emissivities/absorptivities, we construct a triangular based prism. The aspect ratio covers the range of about 0.12 to 11.56 following $\zeta = dzh^{-1}$, where h is the height of the triangle ($dx\ \frac{\sqrt{3}}{2}$). dx was chosen to be constant; dz can be calculated from the same aspect ratio intervals used for the rectangular grid, based on the constant dx. It thus provides the

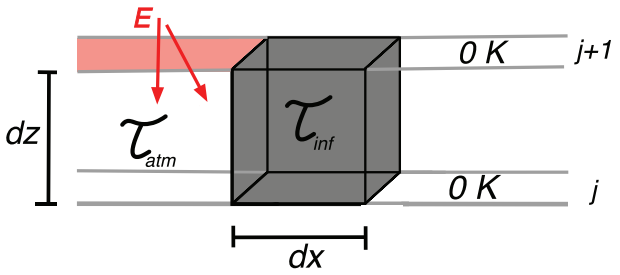

Figure A4. Schematic figure of the MYSTIC setup for the estimation of the side radiance contribution.

analogous aspect ratio range to the rectangular grid. Again, correction factors are calculated for top/base and side contributions to the heating rate separately by following the same idea that either the neighboring atmosphere in the horizontal is assumed to be a black body or the atmosphere directly above and below the triangular based prism, 1,000 per grid box of the prism which again keeps our results stable.

The factors are stored in two lookup tables: one for the top and one for the side correction factors based on the aspect ratio and the optical depth.

Acknowledgments
This project was founded by the German Federal Ministry of Education and Research (BMBF) through the High Definition Clouds and Precipitation for Climate Prediction project (HD(CP)^2) phase 2 (Förderkennzeichen: 01LK1504D and 01LK1507D) and by subproject B4 of the Transregional Collaborative Research Center SFB / TRR 165 "Waves to Weather" (www.wavestoweather.de) funded by the German Research Foundation (DFG). The authors thank Dr. Claudia Emde and Dr. Leonhard Scheck for reading the manuscript and helpful discussion. The NCA is part of libRadtran (www.libradtran.org) and will be included in the next release of libRadtran at the end of 2019. Data sources are described in the text. The lookup tables and data to reproduce the figures are available via: DOI: 10.5282/ubm/data.171. We thank the two anonymous reviewers for their time and effort. Their comments were gratefully received and helped us to improve the paper.

References

Anderson, G. P., Clough, S. A., Kneizys, F. X., Chetwynd, J. H., & Shettle, E. P. (1986). AFGL atmospheric constituent profiles (0-120 km) (*AFGL-TR-86-0110*). Hanscom AFB, MA 01736: AFGL (OPI).

Bretherton, C. S., & Blossey, P. N. (2017). Understanding mesoscale aggregation of shallow cumulus convection using large-eddy simulation. *Journal of Advances in Modeling Earth Systems*, *9*, 2798–2821. https://doi.org/10.1002/2017MS000981

Chandrasekhar, S. (1950). *Radiative transfer*. London, UK: Oxford Univ. Press.

Dipankar, A., Stevens, B., Heinze, R., Moseley, C., Zängl, G., Giorgetta, M., & Brdar, S. (2015). Large eddy simulation using the general circulation model icon. *Journal of Advances in Modeling Earth Systems*, *7*, 963–986. https://doi.org/10.1002/2015MS000431

Emde, C., Buras-Schnell, R., Kylling, A., Mayer, B., Gasteiger, J., Hamann, U., et al. (2016). The libRadtran software package for radiative transfer calculations (version 2.0.1). *Geoscientific Model Development*, *9*(5), 1647–1672.

Evans, K. F. (1998). The spherical harmonics discrete ordinate method for three-dimensional atmospheric radiative transfer. *Journal of the Atmospheric Sciences*, *55*, 429–446.

Fu, Q., & Liou, K. N. (1992). On the correlated k-distribution method for radiative transfer in nonhomogeneous atmospheres. *Journal of the Atmospheric Sciences*, *49*, 2139–2156.

Guan, H., Yau, M. K., & Davies, R. (1997). The effects of longwave radiation in a small cumulus cloud. *Journal of the Atmospheric Sciences*, *54*, 2201–2214.

Heinze, R., Dipankar, A., Henken, C. C., Moseley, C., Sourdeval, O., Trömel, S., et al. (2017). Large-eddy simulations over germany using icon: a comprehensive evaluation. *Quarterly Journal of the Royal Meteorological Society*, *143*(702), 69–100.

Jakub, F., & Mayer, B. (2015a). A three-dimensional parallel radiative transfer model for atmospheric heating rates for use in cloud resolving models—The TenStream solver. *Journal of Quantitative Spectroscopy and Radiative Transfer*, *163*(0), 63–71.

Jakub, F., & Mayer, B. (2015b). 3-D radiative transfer in large-eddy simulations—Experiences coupling the TenStream solver to the UCLAâĂŞLES. *Geoscientific Model Development Discussions*, *8*(10), 9021–9043.

Kablick, G. P. III, Ellingson, R. G., Takara, E. E., & Gu, J. (2011). Longwave 3D benchmarks for inhomogeneous clouds and comparisons with approximate methods. *Journal of Climate*, *24*, 2192–2205.

Khairoutdinov, M. F., & Randall, D. A. (2003). Cloud resolving modeling of the arm summer 1997 iop: Model formulation, results, uncertainties, and sensitivities. *Journal of the Atmospheric Sciences*, *60*(4), 607–625.

Kirchhoff, G. (1890). Über das Verhältniss zwischen dem Emissionsvermögen und dem Absorptionsvermögen der Körper fuer Wärme und Licht. *Annalen der Physik und Chemie*, *109*, 275–301.

Klinger, C., Feingold, G., & Yamaguchi, T. (2019). Cloud droplet growth in shallow cumulus clouds considering 1-d and 3-d thermal radiative effects. *Atmospheric Chemistry and Physics*, *19*(9), 6295–6313.

Klinger, C., & Mayer, B. (2014). Three-dimensional Monte Carlo calculation of atmospheric thermal heating rates. *Journal of Quantitative Spectroscopy and Radiative Transfer*, *144*, 123–136.

Klinger, C., & Mayer, B. (2016). The Neighboring Column Approximation (NCA)—A fast approach for the calculation of 3D thermal heating rates in cloud resolving models. *Journal of Quantitative Spectroscopy and Radiative Transfer*, *168*, 17–28.

Klinger, C., Mayer, B., Jakub, F., Zinner, T., Park, S.-B., & Gentine, P. (2017). Effects of 3-d thermal radiation on the development of a shallow cumulus cloud field. *Atmospheric Chemistry and Physics*, *17*(8), 5477–5500.

Liou, K. N. (2002). *An introduction to atmospheric radiation*, International Geophysics, vol. 84. San Diego: Academic Press.

Mayer, B. (2009). Radiative transfer in the cloudy atmosphere. *European Physical Journal Conferences*, *1*, 75–99.

Mayer, B., & Kylling, A. (2005). Technical Note: The libRadtran software package for radiative transfer calculations: Description and examples of use. *Atmospheric Chemistry and Physics*, *5*, 1855–1877.

Naumann, A. K., Stevens, B., Hohenegger, C., & Mellado, J. P. (2017). A conceptual model of a shallow circulation induced by prescribed low-level radiative cooling. *Journal of the Atmospheric Sciences*, *74*(10), 3129–3144.

Planck, M. (1901). Über das Gesetz der Energieverteilung im Normalspektrum. *Annalen der Physik*, *4*, 533 ff.

Seifert, A., Heus, T., Pincus, R., & Stevens, B. (2015). Large-eddy simulation of the transient and near-equilibrium behavior of precipitating shallow convection. *Journal of Advances in Modeling Earth Systems*, *7*, 1918–1937. https://doi.org/10.1002/2015MS000489

Stevens, B., Moeng, C., Ackerman, A., Bretherton, C., Chlond, A., De Roode, S., et al. (2005). Evaluation of large-eddy simulations via observations of nocturnal marine stratocumulus. *Monthly Weather Review*, *133*, 1443–1462.

van der Dussen, J. J., de Roode, S. R., Ackerman, A. S., Blossey, P. N., Bretherton, C. S., Kurowski, M. J., et al. (2013). The GASS/EUCLIPSE model intercomparison of the stratocumulus transition as observed during ASTEX: LES results. *Journal of Advances in Modeling Earth Systems*, *5*(3), 483–499. https://doi.org/10.1002/jame.20033

Wood, R. (2012). Stratocumulus clouds. *Monthly Weather Review*, *140*(8), 2373–2423.